Talanta 120 (2014) 64–70

Contents lists available at ScienceDirect

Talanta

journal homepage: www.elsevier.com/locate/talanta

Analysis of explosives using corona discharge ionization combined with ion mobility spectrometry–mass spectrometry

Jihyeon Lee [a], Sehwan Park [a], Soo Gyeong Cho [b], Eun Mee Goh [b], Sungman Lee [c], Sung-Suk Koh [c], Jeongkwon Kim [a,*]

[a] Department of Chemistry, Chungnam National University, Daejeon, Republic of Korea
[b] Agency for Defense Development, Daejeon 305-600, Republic of Korea
[c] Sensor Tech Inc., Kyunggi-Do 462-713, Republic of Korea

ARTICLE INFO

Article history:
Received 16 October 2013
Received in revised form
20 November 2013
Accepted 21 November 2013
Available online 28 November 2013

Keywords:
Explosives
Corona discharge ionization
Ion mobility spectrometry
Mass spectrometry

ABSTRACT

Corona discharge ionization combined with ion mobility spectrometry–mass spectrometry (IMS–MS) was utilized to investigate five common explosives: cyclonite (RDX), trinitrotoluene (TNT), pentaerythritol tetranitrate (PETN), cyclotetramethylenetetranitramine (HMX), and 2,4-dinitrotoluene (DNT). The MS scan and the selected ion IMS analyses confirmed the identities of the existing ion species and their drift times. The ions observed were $RDX \cdot NO_3^-$, TNT^-, $PETN \cdot NO_3^-$, $HMX \cdot NO_3^-$, and DNT^-, with average drift times of 6.93 ms, 10.20 ms, 9.15 ms, 12.24 ms, 11.30 ms, and 8.89 ms, respectively. The reduced ion mobility values, determined from a standard curve calculated by linear regression of $(\text{normalized drift times})^{-1}$ versus literature K_0 values, were 2.09, 1.38, 1.55, 1.15, 1.25, and 1.60 $cm^2\,V^{-1}\,s^{-1}$, respectively. The detection limits were found to be 0.1 ng for RDX, 10 ng for TNT, 0.5 ng for PETN, 5.0 ng for HMX, and 10 ng for DNT. Simplified chromatograms were observed when nitrogen, as opposed to air, was used as the drift gas, but the detection limits were approximately 10 times worse (i.e., less sensitivity of detection).

1. Introduction

Ion mobility spectrometry (IMS) is frequently used for the detection of explosives, illegal drugs, and chemical warfare agents [1,2] because it uses equipment that is small and simple to operate. The most common ionization source for the analysis of explosives by IMS is radioactive ^{63}Ni, used to ionize explosive vapors [1]. However, the health risks of ^{63}Ni, as well as low ion signals, have led many researchers to investigate other ionization techniques for analyzing explosives. Two alternatives to ^{63}Ni as an ionization source are corona discharge and secondary electrospray ionization (for a review, see [3]). Corona discharge provides an approximately 100-fold greater electron current than ^{63}Ni [4]. Recently, corona discharge ionization was coupled with IMS to analyze explosives [4–6].

Mass spectrometry (MS) is popularly used to analyze explosives because of its accuracy in identifying explosives from the *m/z* values [7]. Several groups have attempted to combine IMS with MS (IMS–MS) for the analysis of explosives [3,8–10]. IMS–MS is a powerful technique because it determines ion mobility and *m/z* values simultaneously. In the current study, corona discharge ionization combined with IMS–MS was used to examine five explosives: cyclonite (RDX), trinitrotoluene (TNT), pentaerythritol tetranitrate (PETN), cyclotetramethylenetetranitramine (HMX), and 2,4-dinitrotoluene (DNT).

2. Experimental

2.1. Materials and chemicals

RDX, TNT, PETN, HMX, and DNT, shown in Fig. 1, were obtained from the Agency for Defense Development (Daejeon, Korea). Acetonitrile (ACN), used as the solvent, was purchased from Sigma-Aldrich (St. Louis, MO, USA).

2.2. Instrument

IMS–MS was performed using an RA4100 ion mobility spectrometer (Excellims, Acton, MA, USA) equipped with quadrupole MS and corona discharge ionization in negative ion mode. The operating conditions were as follows: source voltage, −10.9 kV; drift tube voltage, −8.9 kV; gate width, 70 μs; and temperature of the desorber and drift tube, 180 °C. The drift length, or the distance from the gate to the detector, was 10.5 cm. Details of the drift tube have been published by Excellims [11]. Purified dry air was used as the drift gas in most of the experiments, although some experiments used nitrogen gas for comparison.

* Correspondence to: Department of Chemistry, Chungnam National University, 99 Daehak-Ro, Yuseong-Gu, Daejeon 305-764, Republic of Korea.
Tel.: 82 42 821 5477; fax: 82 42 821 8896.
E-mail address: jkkim48105@cnu.ac.kr (J. Kim).

0039-9140/$ - see front matter © 2013 Elsevier B.V. All rights reserved.
http://dx.doi.org/10.1016/j.talanta.2013.11.059

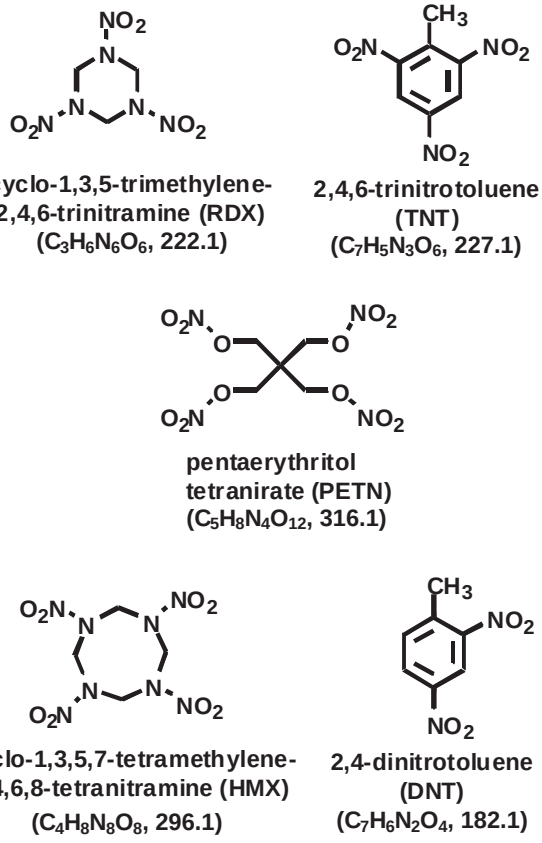

Fig. 1. Structures of the five explosives investigated in this study.

2.3. Sample preparation

Stock solutions were prepared by dissolving each explosive in ACN to a concentration of 10 mg/mL. Aliquots of the stock solutions were then serially diluted with ACN to provide sample solutions at concentrations of 0.1, 0.5, 1.0, 5.0, 10.0, 50.0, 100, 500, and 1000 μg/mL. Finally, 1.0 μL of each sample solution was deposited onto a Nomex swab (Excellims, part number 1002252.03), which was then introduced into the desorption port of the spectrometer after the solvent had evaporated. For qualitative analysis, the sample concentration of 100 μg/mL was used unless otherwise specified.

2.4. Description of procedure

The drift time for each explosive was acquired for 20 ms. The acquisition time for the chromatogram was set to 40 s. A Faraday detector was used to determine the drift time. To determine the *m/z* value for each explosive, the MS scan mode was used with a scan range of *m/z* 50–*m/z* 500. To identify the drift time of a specific ion with a certain *m/z* value, the selected ion IMS was used, whereby the quadrupole was set to pass the specific *m/z* ion while the drift time was acquired by the Faraday detector.

3. Results and discussion

3.1. Identification of the peaks

3.1.1. Analysis of air

To investigate whether air without any sample would provide any signals, an empty swab was introduced to the IMS–MS. Fig. 2A shows the ion mobility spectrum of the empty swab. The mass spectrum showed three distinctive peaks at *m/z* 60, *m/z* 62, and *m/z* 125, as shown in the inset of Fig. 2A. Negative corona discharge of air at ambient pressure generates the CO_3^- ion at *m/z* 60 [12], NO_3^- ion at *m/z* 62 [13], and $HNO_3 \cdot NO_3^-$ at *m/z* 125 [14]. The mass-selected IMS spectrum obtained for the three candidate ions confirmed the drift times of the three ions at 5.79 ms for CO_3^-, 6.00 ms for NO_3^-, and 6.94 ms for $HNO_3 \cdot NO_3^-$ (Fig. 2B). In the mass-selected IMS spectrum for *m/z* 62 of NO_3^-, two major peaks were observed at 6.00 ms and 6.94 ms; the peak at 6.94 ms is believed to be from the fragmentation of $HNO_3 \cdot NO_3^-$.

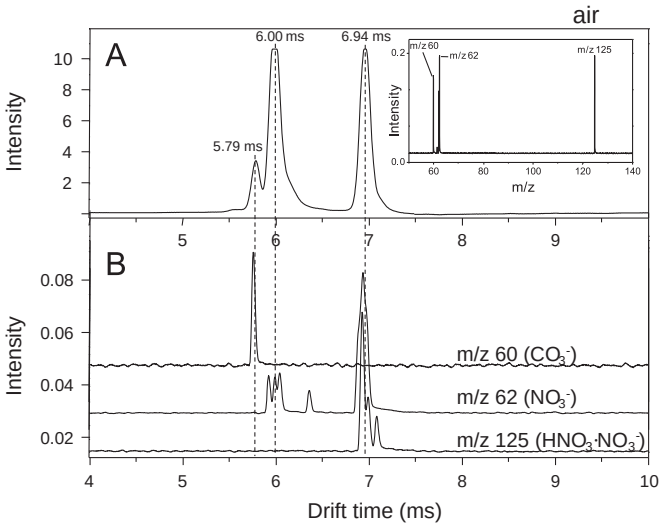

Fig. 2. IMS–MS analysis of air. (A) Ion mobility spectrum and (B) mass-selected ion mobility spectra of CO_3^- at *m/z* 60, NO_3^- at *m/z* 62, and $HNO_3 \cdot NO_3^-$ at *m/z* 125. The inset of (A) shows the mass spectrum from *m/z* 50 to *m/z* 140.

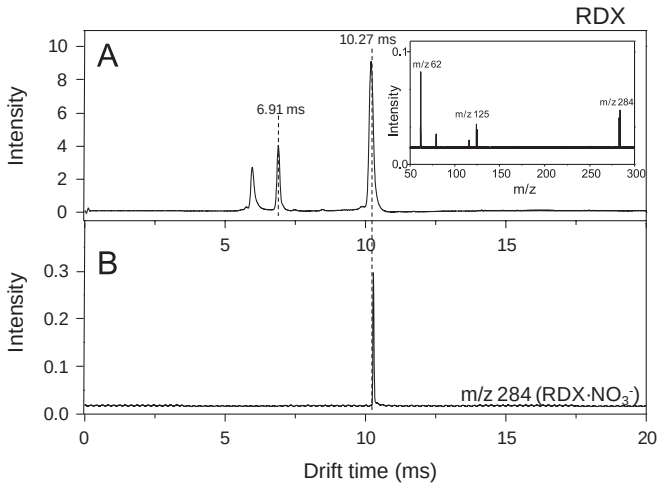

Fig. 3. IMS–MS analysis of 100 ng RDX. (A) Ion mobility spectrum and (B) mass-selected ion mobility spectrum of $[RDX \cdot NO_3]^-$ at *m/z* 284. The inset of (A) shows the mass spectrum from *m/z* 50 to *m/z* 300.

3.1.2. Analysis of RDX

Fig. 3 shows the ion mobility spectrum of 100 ng RDX. The drift time was 10.27 ms (Fig. 3A). The MS scan (inset) and the selected ion IMS analysis (Fig. 3B) showed that RDX was observed as a nitrate adduct ($RDX \cdot NO_3^-$) at *m/z* 284. RDX has been previously observed as $RDX \cdot NO_3^-$ using corona discharge ionization [3].

3.1.3. Analysis of TNT

Fig. 4 shows the ion mobility spectrum of 100 ng TNT. The drift time was 9.25 ms (Fig. 4A). The MS scan (inset) and the mass-selected

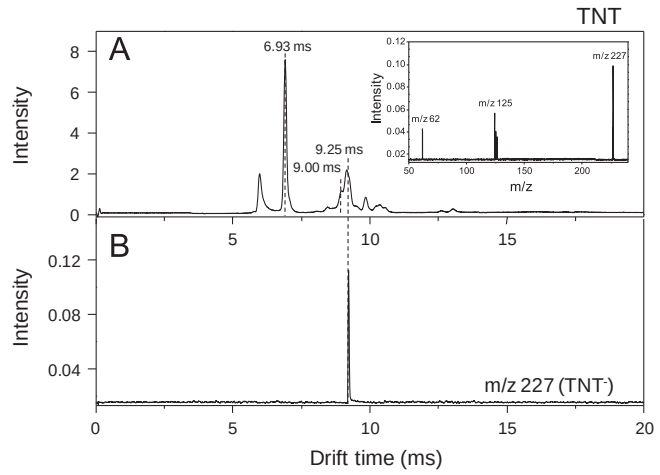

Fig. 4. IMS–MS analysis of 100 ng TNT. (A) Ion mobility spectrum and (B) mass-selected ion mobility spectrum of $[TNT]^-$ at *m/z* 227. The inset of (A) shows the mass spectrum from *m/z* 50 to *m/z* 240.

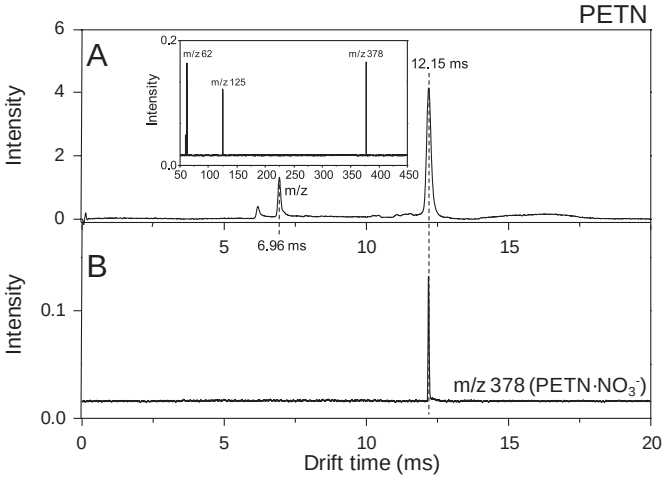

Fig. 5. IMS–MS analysis of 100 ng PETN. (A) Ion mobility spectrum and (B) mass-selected ion mobility spectrum of $[PETN \cdot NO_3]^-$ at *m/z* 378. The inset of (A) shows the mass spectrum from *m/z* 50 to *m/z* 450.

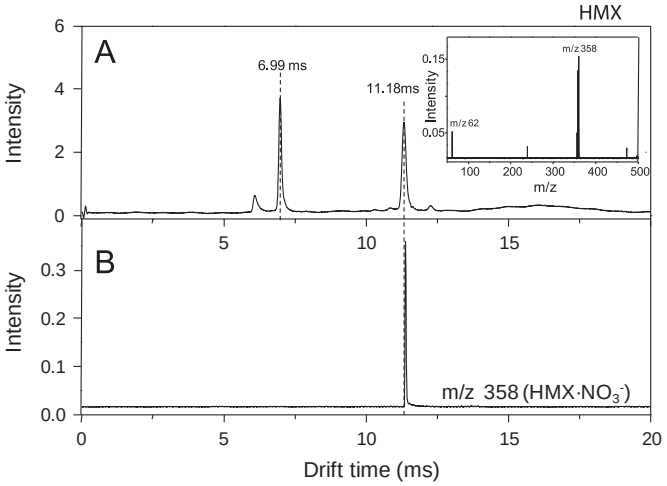

Fig. 6. IMS–MS analysis of 100 ng HMX. (A) Ion mobility spectrum and (B) mass-selected ion mobility spectrum of $[HMX \cdot NO_3]^-$ at *m/z* 358. The inset of (A) shows the mass spectrum from *m/z* 50 to *m/z* 500.

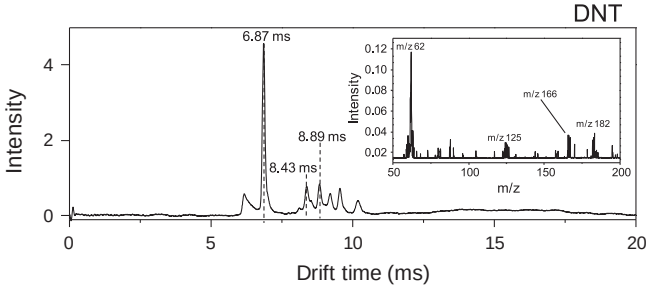

Fig. 7. Ion mobility spectrum of 1000 ng DNT, with the inset showing the mass spectrum from *m/z* 50 to *m/z* 200.

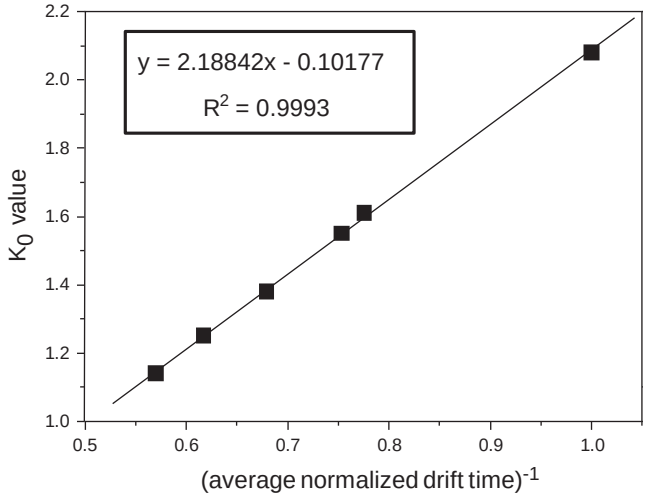

Fig. 8. Relationship between $(\text{normalized drift times})^{-1}$ and K_0 values from the literature. The result of the linear regression was used to calculate the K_0 values of the explosives.

Table 1
Summary of drift times and normalized drift times of ion species.

Ion species	Average	SD[a]	%RSD[b]	*N*[c]
$HNO_3 \cdot NO_3^-$				
Drift time (ms)	6.93	0.07	1.0%	222
Normalized drift time[d]	1.000	0.000	0.0%	
$RDX \cdot NO_3^-$				
Drift time (ms)	10.20	0.16	1.5%	41
Normalized drift time[d]	1.472	0.004	0.3%	
TNT^-				
Drift time (ms)	9.15	0.07	0.7%	58
Normalized drift time[d]	1.327	0.005	0.3%	
$PETN \cdot NO_3^-$				
Drift time (ms)	12.24	0.05	0.4%	45
Normalized drift time[d]	1.754	0.003	0.2%	
$HMX \cdot NO_3^-$				
Drift time (ms)	11.30	0.04	0.3%	32
Normalized drift time[d]	1.620	0.003	0.2%	
DNT^-				
Drift time (ms)	8.89	0.09	1.0%	46
Normalized drift time[d]	1.289	0.003	0.2%	

[a] Standard deviation.
[b] Percent relative standard deviation.
[c] Number of measurements.
[d] Obtained by dividing the drift time of each ion species by the drift time of $HNO_3 \cdot NO_3^-$ in the same spectrum.

IMS analysis (Fig. 4B) showed that TNT was observed as TNT^- at *m/z* 227. TNT has been previously observed as TNT^- using corona discharge ionization [15,16] but has also been reported as $[TNT–H]^-$ [17].

We assume the peak at 9.25 ms is from TNT^- and the shoulder peak at 9.00 ms is from $[TNT–H]^-$ because the mobility $[TNT–H]^-$ is greater than that of TNT^- [18].

3.1.4. Analysis of PETN

Fig. 5 shows the ion mobility spectrum of 100 ng PETN. The drift time was 12.15 ms (Fig. 5A). The MS scan (inset) and the mass-selected IMS analysis (Fig. 5B) showed that PETN was observed as a nitrate adduct ($PETN \cdot NO_3^-$) at *m/z* 378. PETN was previously observed as $PETN \cdot NO_3^-$ using corona discharge ionization [3,19].

3.1.5. Analysis of HMX

Fig. 6 shows the ion mobility spectrum of 100 ng HMX. The drift time was 11.18 ms (Fig. 6A). The MS scan (inset) and the mass-selected IMS analysis (Fig. 6B) showed that HMX was observed as a nitrate adduct ($HMX \cdot NO_3^-$) at *m/z* 358. HMX has been observed as $HMX \cdot NO_3^-$ when low-temperature plasma ambient ionization was used to ionize HMX [20]. HMX was detected as $HMX \cdot HCOO^-$ or $HMX \cdot Cl^-$ using electrospray ionization (ESI)–MS [21] and as $HMX \cdot NO^-$ or $HMX \cdot NO_2^-$ using electron impact ionization and chemical ionization [22]. The extremely low vapor pressure of HMX may explain why HMX has not been readily characterized [23].

3.1.6. Analysis of DNT

Fig. 7 shows the ion mobility spectrum of 1000 ng DNT. The drift times were 8.19 ms, 8.43 ms, 8.89 ms (major), 9.27 ms, and 9.62 ms. The MS scan analysis of DNT (inset) showed two distinct peaks at *m/z* 166 and *m/z* 182. The peak at *m/z* 182 is believed to be from DNT^-. However, we could not confidently assign the mass spectral peaks to peaks in the ion mobility chromatograph because no mass-selected ion mobility spectrum was obtained for any of the masses. We assume the peak with a drift time of 8.89 ms is from the mass of *m/z* 182. This assumption seems reasonable

Table 2
Summary of *m/z* values, normalization, and calculated K_0 values for the observed ions.

Sample	Observed ion	Observed *m/z* value	Observed average t_d (ms)	Average normalized t_d	(Average normalized t_d)$^{-1}$	Calculated K_0 ($cm^2\,V^{-1}\,s^{-1}$)[a]	K_0 from literature ($cm^2\,V^{-1}\,s^{-1}$)[b]
Air	$HNO_3 \cdot NO_3^-$	125	6.93	1.000	1.000	2.09	2.07[6][c,d], 2.08[31][e],
RDX	$RDX \cdot NO_3^-$	284	10.20	1.472	0.679	1.38	1.35[32][c,f], 1.38[3][d], 1.436[30][c,d], 1.46[6][c,d]
TNT	TNT^-	227	9.15	1.327	0.754	1.55	1.49[29][g], 1.55[4][c,d], 1.55[5][c,d]
PETN	$PETN \cdot NO_3^-$	378	12.24	1.754	0.570	1.15	1.10[19][c,d], 1.14[32][c,h], 1.16[3][d], 1.21[4][c,d]
HMX	$HMX \cdot NO_3^-$	357	11.30	1.620	0.617	1.25	1.25[8][c,f]
DNT	DNT^-	182	8.89	1.289	0.776	1.60	1.61[29][g], 1.67[10][g]

[a] Calculated using a linear regression curve of (average normalized t_d)–1 versus K_0 values from the literature.
[b] Values used for generating the linear regression curve are underlined.
[c] No mass spectral identification performed.
[d] Observed with corona discharge ionization.
[e] Observed in the analysis of hexamethylene triperoxide diamine using a ^{63}Ni ion source.
[f] Observed using electrospray ionization.
[g] Observed using a ^{63}Ni ion source.
[h] Observed using secondary electrospray ionization.

Table 3
Peak intensities of the explosives at different injection amounts and the detection limits in the current study along with values from the literature.

Concentration (μg/mL)	RDX	TNT	PETN	HMX	DNT
Intensity values of different explosives[a]					
0.1	0.26 (±0.03)	–[b]	–[b]	–[b]	–[b]
0.5	0.92 (±0.14)	–[b]	0.26 (±0.05)	–[b]	–[b]
1	1.31 (±0.05)	0.06 (±0.01)	0.47 (±0.03)	–[b]	–[b]
5	5.02 (±0.22)	0.81 (±0.19)	1.48 (±0.08)	0.24 (±0.02)	–[b]
10	6.93 (±0.43)	1.61 (±0.31)	2.40 (±0.22)	0.37 (±0.02)	0.27 (±0.06)
50	10.19 (±0.37)	3.36 (±0.51)	4.24 (±0.18)	1.99 (±0.04)	0.61 (±0.02)
100	SA[c]	3.82 (±0.18)	5.08 (±0.05)	3.16 (±0.10)	1.09 (±0.09)
500	SA[c]	7.69 (±0.30)	5.90 (±0.17)	8.68 (±0.07)	3.03 (±0.17)
1000	SA[c]	8.29 (±0.07)	5.33 (±0.04)	10.00 (±0.14)	3.80 (±0±.05)
Detection limits					
Current corona discharge-IMS (μg/mL) or (ng)[d]	0.1	1.0	0.5	5.0	10
ESI–IMS (μg/mL)[8]	0.04	0.015	–[e]	0.086	0.026
DESI–MS (ng)[26]	0.01	0.001	0.1	0.01	–[e]
LTP–MS at room temperature (ng)[20]	0.08	0.08	0.4	60	0.15
LTP–MS at 120 °C (ng)[20]	0.03	0.0006	0.06	0.6	0.005
SFC–APCI–MS (ng)[27]	1635	2912	598	1115	143[f]

[a] Standard deviation values (in parentheses) were obtained with $n=3$.
[b] Not detected.
[c] Detector saturated.
[d] The units of μg/mL and ng are interchangeable since 1 μL sample was used for the analysis.
[e] Not reported.
[f] Data is for 2,6-DNT.

given the correlation between our experimental drift value and the literature K_0 values. The details are explained in Section 3.3. Calculation of reduced mobility values. DNT has been observed as DNT^- using laser desorption followed by ^{63}Ni-induced ion–molecule interactions [10]. With electrospray ionization in negative ion mode, DNT was observed as $[DNT–H]^-$ [8].

3.2. Normalization of drift times

We often observed that the drift time would gradually change as the experiments were performed. To consider the effect of changing drift times between runs, we introduced a new concept of a normalized drift time. Since the peak from $HNO_3 \cdot NO_3^-$ was constantly observed in all experiments, normalized drift times were obtained by dividing the drift time of the explosive by the drift time of $HNO_3 \cdot NO_3^-$ in the same ion mobility spectrum. Thus, the $HNO_3 \cdot NO_3^-$ peak was used as an internal standard. Table 1 shows the comparison of the drift times and the normalized drift times. The percent relative standard deviation (%RSD) of the normalized drift times was significantly less than that of the drift times.

3.3. Calculation of reduced mobility values

Mobility of an ion in IMS is disproportional to the drift time of the ion and can be calculated as follows:

$$K = \frac{L^2}{V t_d} \quad (1)$$

where K is the mobility ($cm^2\,V^{-1}\,s^{-1}$), L is the length of the drift tube (cm), V is the applied potential (V), and t_d is the drift time of the ion(s). To compensate for the environmental variations, the reduced mobility (K_0), which is defined as follows, is frequently used,

$$K_0 = K\left(\frac{P}{760}\right)\left(\frac{273}{T}\right) \quad (2)$$

where P is the pressure in the drift region (mm Hg) and T is the temperature of the drift tube in Kelvin (K) [3,9,24].

The K_0 values of the five explosives under our experimental conditions were determined from a standard curve calculated by linear regression of a plot of (average normalized $t_d)^{-1}$ versus literature K_0 values. The linear regression curve is shown in Fig. 8. Based on Eqs. (1) and (2), K_0 is proportional to $1/t_d$. Since the normalized t_d accounts for any inaccuracy in the drift times, we used normalized t_d. Table 2 shows the ion species, m/z values, drift times, normalized drift times, K_0 values obtained from the linear regression curve, and K_0 values from the literature. In the case of HMX, we were unable to find any reported K_0 value for $HMX \cdot NO_3^-$. Our K_0 values for the ions adducted with Cl^- or NO_3^- were in agreement with reported K_0 values. For example, the K_0 values of $RDX \cdot Cl^-$ and $PETN \cdot Cl^-$ were reported to be 1.40 $cm^2\,V^{-1}\,s^{-1}$ [8] and 1.15 $cm^2\,V^{-1}\,s^{-1}$ [25], respectively, which agrees with the K_0 values of $RDX \cdot NO_3^-$ and $PETN \cdot NO_3^-$ shown in Table 2. Consequently, the K_0 value of 1.25 $cm^2\,V^{-1}\,s^{-1}$ for $HMX \cdot Cl^-$ is listed in place of $HMX \cdot NO_3^-$ in Table 2. The R^2 value for the plot of (average normalized $t_d)^{-1}$ and literature K_0 values was found to be 0.9993. Thus, the calculated K_0 values of the explosives are very close to the literature K_0 values.

3.4. Quantitative analysis

Table 3 summarizes the peak intensity values for the explosives at different concentrations. In each case, the maximum intensity was used as the intensity value. For TNT and DNT, the intensity values of all the peaks were summed together. The detection limits were found to be 0.1 ng for RDX, 10 ng for TNT, 0.5 ng for PETN, 5.0 ng for HMX, and 10 ng DNT. Table 3 also includes detection limits obtained from the literature for ESI–MS [8], desorption electrospray ionization (DESI)–MS [26], low-temperature plasma ionization (LTP)–MS [20], and supercritical fluid chromatography–atmospheric pressure chemical ionization (SFC-APCI)–MS [27]. While RDX was observed with the lowest detection limit of the five explosives in our analysis, in other investigations, TNT was usually observed with the lowest detection limit (for a more thorough review of detection limits of explosives, see [23]).

Fig. 9 shows the relationship between the concentration (0.1^{-1}000 μg/mL) of the explosives and the peak intensity in the IMS analysis; three different plots are presented to clearly illustrate the relationship. Since 1.0 μL was loaded for each experiment, the units of μg/mL and ng are interchangeable. Among the five explosives, the most sensitive detection was observed for RDX. The most rapid increase of the response was observed for small injection amounts (< 50 ng), and an injection of 100 ng saturated the Faraday detector. In the case of PETN, the response increased rapidly and then stabilized in the middle. Gradual increases of response were observed for TNT and HMX. DNT showed the smallest response of the five explosives at all concentrations.

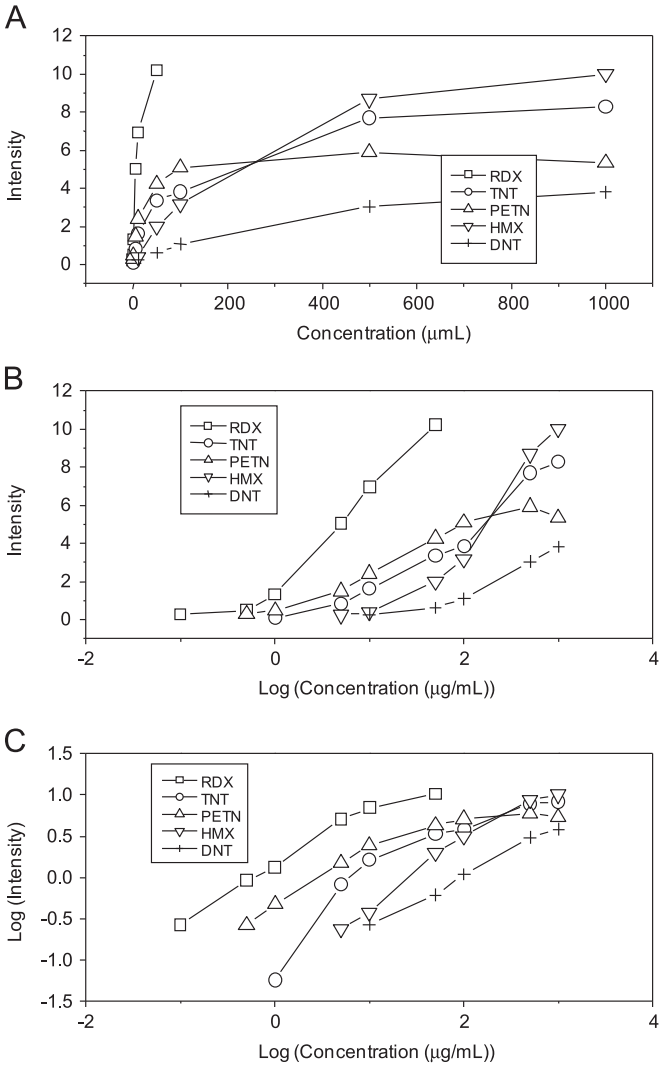

Fig. 9. Relationship between the analyte concentration and the peak intensity in the IMS analysis of five explosives. Three different plots are shown: (A) concentration vs. intensity, (B) log(concentration) vs. intensity, and (C) log (concentration) vs. log(intensity).

3.5. Comparison of drift gases

Both nitrogen and air have been widely used as drift gases in IMS analysis [28]. In the current investigation, most IMS analyses were performed using air as the drift gas. To investigate the effect of different drift gases on the corona discharge ionization–IMS, nitrogen gas was also applied as a drift gas.

Fig. 10 compares the two drift gases. Approximately equal drift times were observed for the explosives in air versus nitrogen, in agreement with a previous report [29]. A slight increase in the drift times of air-generated NO_3^- and $HNO_3 \cdot NO_3^-$ was observed when nitrogen was used as the drift gas. Increased background signals were also observed when nitrogen was the drift gas, which results in a detection limit approximately 10 times worse than that observed when air was the drift gas. However, the chromatogram was simpler with nitrogen as the drift gas. For example, only the TNT^- peak was dominant with nitrogen as the drift gas, whereas TNT^- and $[TNT–H]^-$ peaks were dominant with air as the drift gas (Fig. 10B). For DNT (Fig. 10E), a single sharp peak, believed to be from $[DNT]^-$, was observed using nitrogen as the drift gas, whereas other peaks appeared when air was the drift gas.

With nitrogen as the drift gas, a large peak around 0.13 ms was detected in all chromatograms, while a very small peak was observed with air as the drift gas. This peak is believed to be an electron peak. The initial process of corona discharge is the capture of an electron by an oxygen and nitrogen molecule [30]. When air is used as the drift gas, this process can proceed and induce subsequent cascading reactions. However, when nitrogen is used as the drift gas, this initial process is restricted, providing abundant electrons. These results agree with previous reports showing a large initial peak with nitrogen as the drift gas [4] and a small initial peak with air as the drift gas [6] in ion mobility spectra.

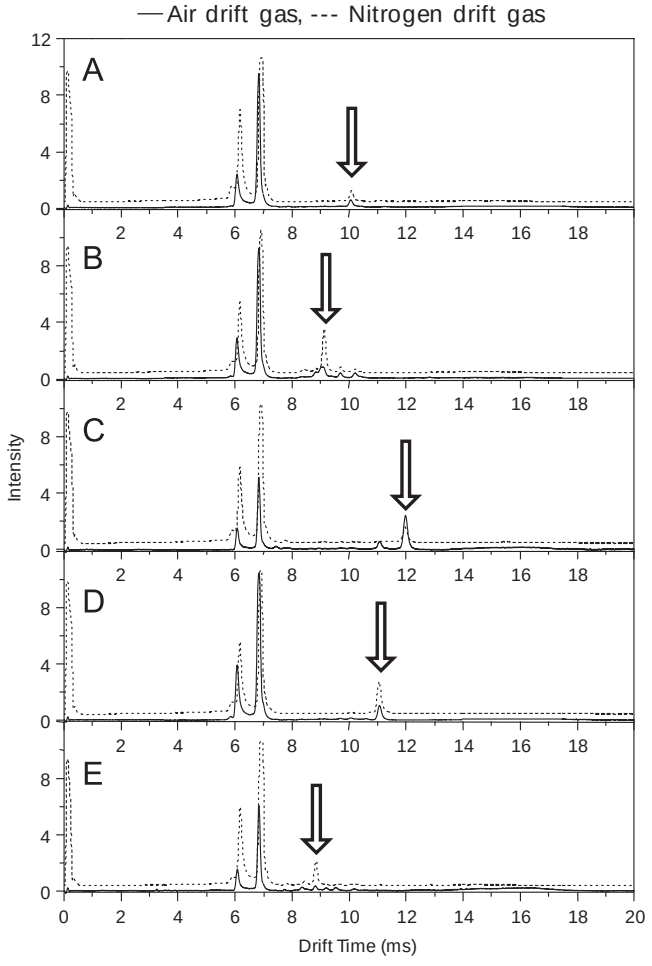

Fig. 10. Effect of air or nitrogen as the drift gas on the drift times of (A) 1 ng RDX, (B) 100 ng TNT, (C) 10 ng PETN, (D) 100 ng HMX, and (E) 100 ng DNT. Solid (—) and dashed (- - -) lines show the chromatograms obtained with air and nitrogen drift gas, respectively.

4. Conclusion

Comprehensive analyses of five explosives were performed using corona discharge ionization IMS–MS. The existing ion species were identified using the MS and selected IMS spectra. The drift times of the explosives were normalized by using the common air peak of $HNO_3 \cdot NO_3^-$ as an internal standard, significantly reducing the relative standard deviations. The smallest and largest detection limits were observed for RDX and DNT, respectively. This differs from other reports using different ionization sources. Even though the current corona discharge ionization is not the best technique in terms of sensitivity in the analysis of explosives, the advantages such as simple operation procedure and inexpensive assembly make the results of this study valuable.

Acknowledgments

This project was financially supported by the Agency for Defense Development.

References

[1] S. Armenta, M. Alcala, M. Blanco, Anal. Chim. Acta 703 (2011) 114–123.
[2] M.A. Mäkinen, O.A. Anttalainen, M.E.T. Sillanpää, Anal. Chem. 82 (2010) 9594–9600.
[3] C.L. Crawford, H.H. Hill, Talanta 107 (2013) 225–232.
[4] T. Khayamian, M. Tabrizchi, M.T. Jafari, Talanta 59 (2003) 327–333.
[5] M. Tabrizchi, A. Abedi, Int. J. Mass Spectrom. 218 (2002) 75–85.
[6] K.M. Roscioli, E. Davis, W.F. Siems, A. Mariano, W.S. Su, S.K. Guharay, H.H. Hill, Anal. Chem. 83 (2011) 5965–5971.
[7] S. Park, J. Lee, S.G. Cho, E.M. Goh, S. Lee, S.-S. Koh, J. Kim, Bull. Korean Chem. Soc. 34 (2013) 3659–3664.
[8] G. Reid Asbury, J. Klasmeier, H.H. HillJr., Talanta 50 (2000) 1291–1298.
[9] J. Kozole, J.R. Stairs, I. Cho, J.D. Harper, S.R. Lukow, R.T. Lareau, R. DeBono, F. Kuja, Anal. Chem. 83 (2011) 8596–8603.
[10] S.D. Huang, L. Kolaitis, D.M. Lubman, Appl. Spectrosc. 41 (1987) 1371–1376.
[11] A.J. Midey, A. Patel, C. Moraff, C.A. Krueger, C. Wu, Talanta 116 (2013) 77–83.
[12] M.M. Shahin, Appl. Opt. 8 (1969) 106–110.
[13] H.E. Manninen, A. Franchin, S. Schobesberger, A. Hirsikko, J. Hakala, A. Skromulis, J. Kangasluoma, M. Ehn, H. Junninen, A. Mirme, S. Mirme, M. Sipila, T. Petaja, D.R. Worsnop, M. Kulmala, Atmos. Meas. Tech. 4 (2011) 2767–2776.
[14] K. Nagato, Y. Matsui, T. Miyata, T. Yamauchi, Int. J. Mass Spectrom. 248 (2006) 142–147.
[15] X. Fu, Y. Zhang, S. Shi, F. Gao, D. Wen, W. Li, Y. Liao, H. Liu, Rapid Commun. Mass Spectrom. 20 (2006) 2906–2914.
[16] K. Kojima, M. Sakairi, Y. Takada, J. Nakamura, J. Mass Spectrom. Soc. Jpn. 48 (2000) 360–362.
[17] J. Laakia, C.S. Pedersen, A. Adamov, J. Viidanoja, A. Sysoev, T. Kotiaho, Rapid Commun. Mass Spectrom. 23 (2009) 3069–3076.
[18] R.G. Ewing, D.A. Atkinson, G.A. Eiceman, G.J. Ewing, Talanta 54 (2001) 515–529.
[19] S.S. Choi, O.B. Kim, Y.K. Kim, S.G. An, M.W. Shin, S.J. Maeng, G.S. Choi, Bull. Korean Chem. Soc. 32 (2011) 1055–1058.
[20] J.F. Garcia-Reyes, J.D. Harper, G.A. Salazar, N.A. Charipar, Z. Ouyang, R.G. Cooks, Anal. Chem. 83 (2011) 1084–1092.
[21] Z. Wu, C.L. Hendrickson, R.P. Rodgers, A.G. Marshall, Anal. Chem. 74 (2002) 1879–1883.
[22] J. Yinon, D.J. Harvan, J.R. Hass, Org. Mass Spectrom. 17 (1982) 321–326.
[23] M. Makinen, M. Nousiainen, M. Sillanpaa, Mass Spectrom. Rev. 30 (2011) 940–973.
[24] C.K. Hilton, C.A. Krueger, A.J. Midey, M. Osgood, J.L. Wu, C. Wu, Int. J. Mass Spectrom. 298 (2010) 64–71.
[25] L.L. Danylewych-May, in: Proceedings of the First International Symposium on Explosive Detection Technology, Atlantic City, NJ, 1991, pp. 672–686.
[26] Z. Takats, I. Cotte-Rodriguez, N. Talaty, H. Chen, R.G. Cooks, Chem. Commun. (2005) 1950–1952.

[27] Y. McAvoy, K. Dost, D.C. Jones, M.D. Cole, M.W. George, G. Davidson, Forensic Sci. Int. 99 (1999) 123–141.
[28] L.M. Matz, H.H. Hill Jr., L.W. Beegle, I. Kanik, J. Am., Soc. Mass Spectrom. 13 (2002) 300–307.
[29] G.E. Spangler, P.A. Lawless, Anal. Chem. 50 (1978) 884–892.
[30] R. Ewing, M. Waltman, Int. J. Ion Mobil. Spectrom. 12 (2009) 65–72.
[31] J. Kozole, J. Tomlinson-Phillips, J.R. Stairs, J.D. Harper, S.R. Lukow, R.T. Lareau, H. Boudries, H. Lai, C.S. Brauer, Talanta 99 (2012) 799–810.
[32] M. Tam, H.H. Hill, Anal. Chem. 76 (2004) 2741–2747.